

1 **Incorporation of technetium into spinel ferrites**

2

3 Wayne W. Lukens,^{1*} Nicola Magnani,^{1,2} Tolek Tyliszczak,³ Carolyn I. Pearce,⁴ David K. Shuh¹

4

5 1) Chemical Sciences Division, Lawrence Berkeley National Laboratory, Berkeley, CA
6 94720

7 2) European Commission, Joint Research Centre, Institute for Transuranium Elements,
8 Karlsruhe

9 3) Advanced Light Source, Lawrence Berkeley National Laboratory, Berkeley, CA 94720

10 4) Geosciences Group, Pacific Northwest National Laboratory, Richland, WA 99354

11

12 * MS 70A-1150, Lawrence Berkeley National Laboratory, Berkeley, CA 94720. Phone (510)
13 486-4305; Fax (510) 486-5596. WWLukens@lbl.gov.

14

15 **Abstract**

16 Technetium (⁹⁹Tc) is a problematic fission product for the long-term disposal of nuclear waste
17 due to its long half-life, high fission yield, and to the environmental mobility of pertechnetate,
18 the stable species in aerobic environments. One approach to preventing ⁹⁹Tc contamination is
19 using sufficiently durable waste forms. We report the incorporation of technetium into a family
20 of synthetic spinel ferrites that have environmentally durable natural analogs. A combination of
21 X-ray diffraction, X-ray absorption fine structure spectroscopy and chemical analysis reveals that
22 Tc(IV) replaces Fe(III) in octahedral sites and illustrates how the resulting charge mismatch is
23 balanced. When a large excess of divalent metal ions is present, the charge is predominantly

24 balanced by substitution of Fe(III) by M(II). When a large excess of divalent metal ions is
25 absent, the charge is largely balanced by creation of vacancies among the Fe(III) sites
26 (maghemitization). In most samples, Tc is present in Tc-rich regions rather than being
27 homogeneously distributed.

28

29 **Introduction**

30 Technetium (^{99}Tc) is a problematic fission product for nuclear waste disposal due to its long
31 half-life (211,000 yr), high fission yield (6 %), and to the environmental mobility of
32 pertechnetate (TcO_4^-), the stable form in aerobic environments.¹⁻⁴ ^{99}Tc migration may be
33 minimized by disposal in an anaerobic repository since Tc(IV) is stable under these conditions
34 and is not highly mobile.³ Alternatively, technetium may be immobilized in a waste form that is
35 sufficiently durable to prevent release of ^{99}Tc until an acceptable fraction has decayed. The
36 current U.S. high-level waste repository is Yucca Mountain, which is aerobic and oxidizing.⁵ In
37 addition, the majority of the ^{99}Tc from plutonium production at the Savannah River and Hanford
38 Sites will be disposed in near-surface, aerobic repositories although the Savannah River Site
39 facility will be reducing initially.^{6,7} Disposal of ^{99}Tc in current and proposed aerobic repositories
40 underscores the interest in durable waste forms for ^{99}Tc .

41

42 Even under reducing conditions, the 3 pM solubility of $\text{TcO}_2 \cdot x\text{H}_2\text{O}$ exceeds the EPA maximum
43 contaminant level of 900 pCi/L or 0.5 pM.⁸⁻¹⁰ Naturally occurring ligands can increase the
44 solubility of Tc(IV).¹¹⁻¹⁴ Therefore, durable waste forms are also desirable for ^{99}Tc disposal in an
45 anaerobic repository. The most commonly used waste form, borosilicate glass, is durable, but
46 loss of volatile technetium species during glass vitrification can make it difficult to retain

47 technetium in the glass.¹⁵⁻¹⁸ Alternatives include synthetic mineral phases, such as Synroc.¹⁹
48 Likewise, certain mineral phases are both highly durable and could accommodate Tc doping.²⁰
49 The similarity of the six coordinate ionic radii of Tc(IV), Ti(IV), and Fe(III), 0.645 Å, 0.604 Å
50 and 0.645 Å,²¹ respectively, suggests that Tc(IV) can replace Ti(IV) or Fe(III) in an oxide
51 mineral.²⁰ Rutile (TiO₂), hematite (α-Fe₂O₃) and goethite (α-FeOOH), are known to be durable
52 under aerobic conditions.²²⁻²⁶ Hematite and goethite are unstable under reducing conditions and
53 could release ⁹⁹Tc; however, migration is slow under these conditions.³ Moreover, Tc(IV) can be
54 incorporated into mineral phases under these conditions as demonstrated by Kobayashi, et al.
55 who showed that prolonged contact of magnetite (Fe₃O₄) with TcO₄⁻ leads to Tc(IV)
56 incorporation.²⁷ Iron oxides, particularly goethite, have received attention as waste forms for
57 stabilizing ⁹⁹Tc.^{28,29} Other iron oxides can also accommodate Tc(IV). Pepper, et al., incorporated
58 Tc(IV) into an iron oxide phase resulting from oxidation of green rust.³⁰ Marshall, et al.
59 demonstrated that adsorption of Tc(IV) onto ferrihydrite followed by conversion to magnetite
60 results in Tc doping.³¹ Tc-doped magnetite has been studied computationally by Smith, et al..³²
61 Lee, et al. demonstrated that Tc(IV) may be incorporated into the lattice of transition metal
62 doped magnetites.¹⁸

63
64 Another family of iron oxides, spinel ferrites (MFe₂O₄, where M is Mg(II), Mn(II), Co(II), or
65 Ni(II)), especially nickel/magnesium ferrite, Mg_xNi_{1-x}Fe₂O₄, are highly durable as evidenced by
66 their persistence since being deposited widely across earth's surface 65 million years ago by the
67 Chixulub meteorite impact.³³ These minerals are inverse spinels, but they will be referred to as
68 "spinel ferrites" for brevity. Synthetic spinel ferrites are attractive potential waste forms for
69 several reasons. Aqueous synthesis conditions and short reaction times (few hours) make them

70 amenable to processing.³⁴⁻³⁸ They are magnetic, potentially allowing magnetic separation of Tc.
71 Incorporation of Tc(IV) into magnetite,^{18,27,31} suggests that other Tc(IV)-doped spinel ferrites
72 may be prepared. This observation leads the hypothesis that starting from TcO_4^- , Tc(IV) will be
73 homogeneously incorporated into spinel ferrites by replacing Fe(III) on M_O sites provided that
74 sufficient Fe(II) is present to reduce TcO_4^- .

75
76 To test the hypothesis and to understand the factors controlling Tc incorporation into spinel
77 ferrites, we have prepared: (i) a series of Tc(IV)-doped spinel ferrites with the composition
78 $\text{Tc}_{0.1}\text{M}_{1.1}\text{Fe}_{1.8}\text{O}_4$, where M is Mn, Co, and Ni; and (ii) a series of magnetites doped with Tc(IV)
79 and divalent metals having the composition $\text{Tc}_{0.1}\text{M}_{0.2}\text{Fe}_{2.7}\text{O}_4$ where M is Mg, Mn, Fe, Co, and
80 Ni. The objectives of this study were (i) to determine whether Tc could be incorporated into the
81 octahedral sites (M_O) of spinel ferrites, $\text{M}_x\text{Fe}_y\text{O}_4$, (ii) to determine the effect of ionic radius of the
82 divalent metal ion, M, on the incorporation of Tc in the spinel ferrite lattice, and (iii) to
83 determine the effect of different synthetic routes on the incorporation of Tc. The two synthetic
84 routes examined were the traditional coprecipitation route (samples indicate by “-c”),³⁴ in which
85 a mixture of M(II), Fe(II) and Fe(III), and TcO_4^- is treated with NaOH to form the ferrite spinel
86 and a oxidation route (samples indicated by “-o”) in which a mixture of M(II), Fe(II) and TcO_4^-
87 is treated with NaOH and NaNO_3 , and Fe(III) is generated *in situ* by oxidation of Fe(II) by NO_3^-

88 .³⁶

89

90 **Experimental Details**

91 **Caution:** ^{99}Tc is β -emitter. All operations were carried out in a laboratory equipped to handle
92 this isotope.

93 **General.** Water was deionized using a Milli-Q Gradient A-10 system. Chemicals were ACS
94 grade or better and were used as received. Fe(II)/total Fe ratios (Fe(II)/ ΣFe) in the spinels were
95 determined colorimetrically.^{39,40} In this method, V(V) is reduced to V(IV) by Fe(II) during
96 dissolution of the sample in acid. When 2,2'-bipyridyl (bipy) and buffer are added, V(IV)
97 quantitatively reduces Fe(bipy) $_3^{3+}$ to red Fe(bipy) $_3^{2+}$, which is measured spectrophotometrically.
98 The Fe(II)/ ΣFe ratios for the Tc-doped samples were decreased proportionally to the amount of
99 Tc recovered from the spinel ferrites and the Tc/Fe ratio to account for reduction of three V(V)
100 by each Tc(IV), e.g., for $\text{Tc}_{0.1}\text{Mn}_{1.1}\text{Fe}_{1.8}\text{O}_{4-o}$ Fe(II)/ ΣFe was decreased by $3 (e^-/\text{Tc(IV)}) \times 0.99$
101 (Tc recovered from solid) $\times 0.1/1.8$ (Tc/Fe). Two sets of independently prepared samples were
102 used for characterization. The initial set was used for XRD and XAFS studies. Later, a second
103 set was prepared for LSC and Fe(II)/Fe(III) measurements to address questions that arose during
104 the analysis of the XRD and XAFS results. Both sets were prepared using the same procedures.

105

106 **Synthesis of Tc-doped spinel ferrites**

107 Note: The stoichiometry of the samples (e.g., " $\text{Tc}_{0.1}\text{Co}_{1.1}\text{Fe}_{1.8}$ ") are based on the amount of each
108 metal added during the synthesis. The samples contain 4 wt% Tc.

109 Two approaches were used to prepare samples: coprecipitation and oxidation. In the
110 coprecipitation approach, TcO_4^- was added to a mixture of divalent metal ion and Fe(III).³⁴ A
111 five-fold excess of Fe(II) relative to TcO_4^- was used to reduce TcO_4^- to Tc(IV). The solution was
112 neutralized with sodium hydroxide and heated. These samples are indicated by a "c" after the

113 formula, e.g., $\text{Tc}_{0.1}\text{Fe}_{2.9}\text{O}_4\text{-c}$. In the oxidation route, TcO_4^- was added to a mixture of Fe(II) and a
114 divalent metal ion; sodium hydroxide and sodium nitrate were added and the solution was
115 heated.³⁶ Fe(III) is formed *in situ* through oxidation of Fe(II) by nitrate, hence the term
116 “oxidation route.” These samples are indicated by an “o” after the formula, e.g., $\text{Tc}_{0.1}\text{Fe}_{2.9}\text{O}_4\text{-o}$.
117 Following the synthesis, the samples were handled and stored in air, and no attempts were made
118 to exclude oxygen.

119
120 **Coprecipitation** (adapted from ref 33). $\text{CoCl}_2\cdot 6\text{H}_2\text{O}$ (53 mg, 0.22 mmol) was dissolved in a
121 mixture of 1.0 M FeSO_4 (0.10 mL, 0.10 mmol) and 1.0 M $\text{NH}_4\text{Fe}(\text{SO}_4)_2$ (0.26 mL, 0.26 mmol).
122 The solution was sparged with argon for 1 minute. A 0.10 M solution of TcO_4^- in 0.03 M HNO_3
123 (200 μL , 0.02 mmol) was added. The headspace of the tube was purged with argon, and the tube
124 was vigorously shaken. Aqueous 2.00 M NaOH (0.91 mL, 1.81 mmol OH^-) was added. The
125 headspace of the tube was purged with argon, and the tube was vigorously shaken. The tube was
126 heated to 95 °C for 90 minutes. After heating, the tube was centrifuged (5 min, 8500 g) and the
127 solution decanted. The black solid was washed with 2×1.5 mL water and 1.5 mL acetone.

128
129 **Oxidation** (adapted from ref. 35). $\text{CoCl}_2\cdot 6\text{H}_2\text{O}$ (53 mg, 0.22 mmol) was dissolved in 1.0 M
130 FeSO_4 (0.36 mL, 0.36 mmol). The solution was sparged with argon for 1 minute. A 0.11 M
131 solution of TcO_4^- in 0.03 M HNO_3 (200 μL , 0.02 mmol) was added. The headspace of the tube
132 was purged with argon, and the tube was vigorously shaken. An aqueous solution of 1.00 M
133 NaNO_3 and 2.00 M NaOH (0.61 mL, 1.21 mmol OH^-) was added. The headspace of the tube was
134 purged with argon, and the tube was vigorously shaken. The tube was heated to 95 °C for 90

135 minutes. After heating, the tube was centrifuged (5 min, 8500 g), and the supernate decanted.
136 The black solid was washed in air with 2×1.5 mL water and 1.5 mL acetone.

137

138 **Synthesis of undoped spinel ferrites.** Samples with the same transition metal composition, but
139 without added Tc were prepared. Both the oxidation synthesis and coprecipitation synthesis were
140 performed as described above except that 200 uL of water was used in place of the NH_4TcO_4
141 solution.

142

143 **Liquid Scintillation Counting (LSC).** Solutions were centrifuged (5 min, 8500 g) to remove
144 Tc-doped ferrite nanoparticles. 100 uL of this solution was added to 4 mL of Ecolume. Samples
145 were analyzed using a Wallac 1414 liquid scintillation counter. Results are not corrected for
146 chemical quench. Comparison of the spectral quench parameter, SQP(E), to a ^{99}Tc quench curve
147 prepared using nitromethane showed that quenching was less than 1%.

148

149 **X-ray diffraction (XRD).** An acetone suspension of the sample was dropped onto a silicon zero
150 background plate. Samples were sealed with Kapton film to control contamination.
151 Diffractograms were recorded using a Panalytical X'Pert Pro diffractometer with a Cu source
152 and a silicon strip detector except for sample $\text{Tc}_{0.1}\text{Ni}_{0.2}\text{Fe}_{2.7}\text{O}_4\text{-c}$, which was recorded using a Co
153 source. Data were summed and analyzed using HiScore Plus software. A blank diffraction
154 pattern from the zero background plate and the Kapton film was subtracted from each diffraction
155 pattern. An empirical background consisting of a curve through the bases of the peaks at low 2θ
156 and through the baseline at high 2θ was removed. The diffraction data were modeled using the

157 crystal structure of magnetite. Rietveld refinement using X'Pert High Score Plus was used to
158 determine the lattice parameters and to estimate the sizes of the crystallites.

159

160 **X-ray absorption fine structure (XAFS) measurements.** Samples were dispersed in acetone or
161 water and centrifuged (5 min, 8500 g), and the liquid was discarded to produce a homogeneous
162 pellet. Data was obtained at room temperature at the Tc K-edge on Beamline 11-2 or 4-1 of the
163 Stanford Synchrotron Radiation Lightsource. Most data were obtained during a single
164 experiment. For samples $\text{Tc}_{0.1}\text{Co}_{1.1}\text{Fe}_{1.8}\text{O}_4\text{-o}$, $\text{Tc}_{0.1}\text{Mg}_{0.2}\text{Fe}_{2.7}\text{O}_4\text{-o}$, and $\text{Tc}_{0.1}\text{Ni}_{0.2}\text{Fe}_{2.7}\text{O}_4\text{-c}$, the
165 pellet dried out and disintegrated inside the centrifuge tube. Spectra from these samples were re-
166 collected during a subsequent experiment using freshly prepared material. X-rays were
167 monochromatized using a double-crystal monochromator with Si [220] $\phi = 90$ crystals; the
168 second crystal was detuned by 70% to reduce the harmonic content of the beam. Spectra were
169 recorded in transmission mode using argon filled ion chambers.

170

171 Data were analyzed by standard procedures⁴¹ using ifeffit⁴² and Artemis/Athena.⁴³ Theoretical
172 scattering curves were calculated using Feff6⁴⁴ based on the structure of titanomagnetite
173 ($\text{Ti}_{0.1}\text{Fe}_{2.9}\text{O}_4$) with Tc in the octahedral site.⁴⁵ Coordination numbers for the neighboring atoms
174 were fixed at the values found in the crystal structure except for the oxygen shell at 2 Å. This
175 shell was split into two shells, one with a short distance (1.5 to 1.75 Å) and another with a longer
176 distance (2 Å); the sum of the oxygen coordination numbers for these shells was fixed at 6, the
177 number of oxygen nearest neighbors for the Ti(IV) site in titanomagnetite. The value of S_0^2 was
178 determined to be 0.80 (rather than 0.90) for fitting the data in this study by fitting several
179 extended X-ray absorption fine structure (EXAFS) spectra of the TcO_4^- reference collected

180 simultaneously with the data. The statistical significance of each scattering shell was evaluated
181 using an F-test.⁴⁶

182

183 **X-ray magnetic circular dichroism spectroscopy (XMCD).** Sample was placed on a 100 nm
184 thick Si₃N₄ window, which was sealed to an identical Si₃N₄ window with epoxy. Data was
185 recorded at the Molecular Environmental Science Beamline 11.0.2 at the Advanced Light Source
186 (ALS) with a scanning transmission X-ray microscope (STXM). XMCD spectra were recorded
187 at the Fe L_{2,3}-edge with the sample in a 0.5 T magnetic field using left and right circularly
188 polarized X-rays from an elliptically polarizing undulator.⁴⁷ Data were recorded as images
189 obtained at different X-ray energies. The background data was obtained from the portion of the
190 image with no sample. Data were pre- and post-edge normalized. Data were fit using nonlinear
191 least-squares analysis with calculated spectra^{48,49} for each site as previously described^{50,51}

192

193 **Results and discussion**

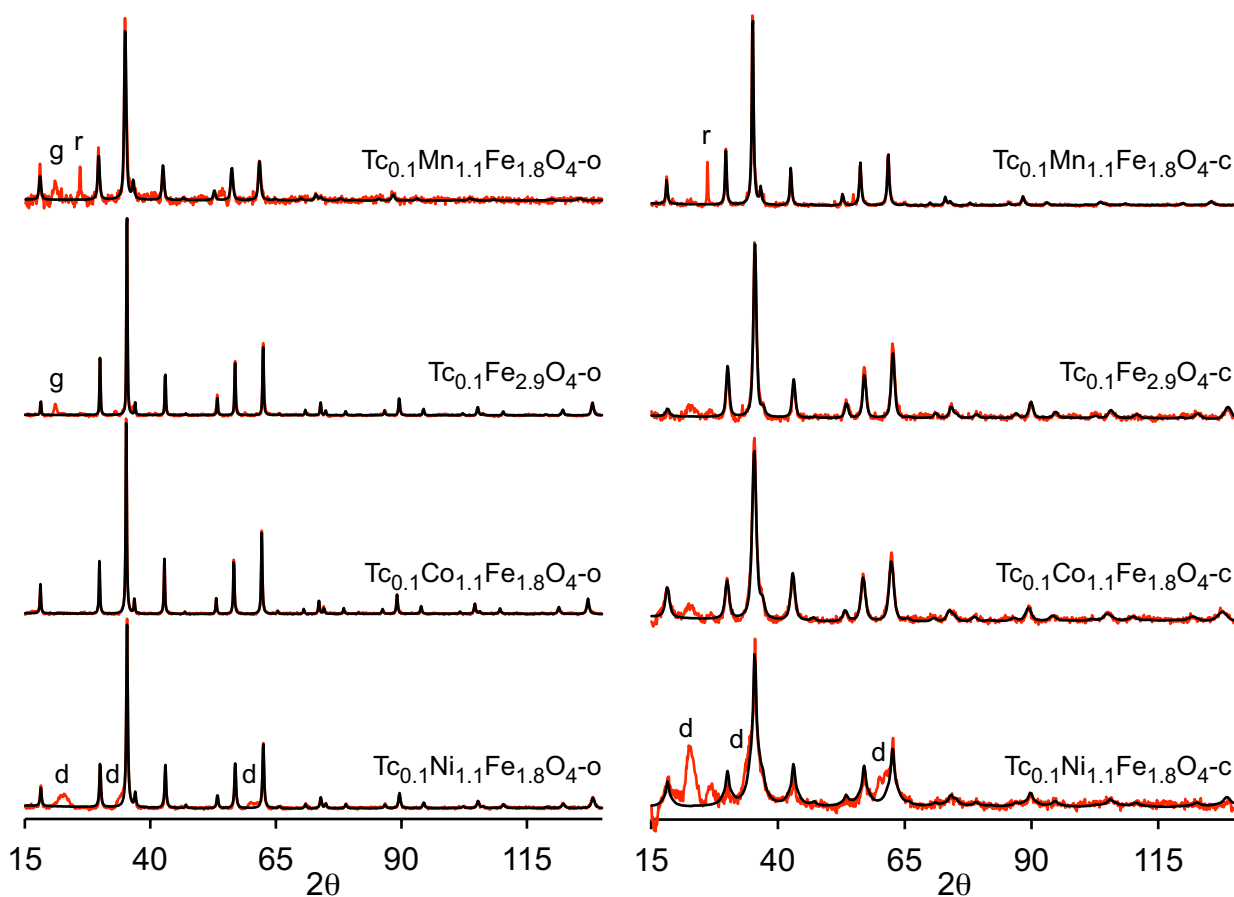
194 **Incorporation of Tc into spinel ferrites.**

195 Incorporation of TcO₄⁻ was evaluated by LSC analysis of the solution remaining after
196 preparation of the spinel ferrite (Table S1). More than 99.5 % of the Tc was removed from
197 solution in all cases; in the oxidation route, more than 99.88 % of the Tc was removed. The Tc
198 remaining in solution is presumably TcO₄⁻. These results are consistent with work by Livens and
199 coworkers using green rust to trap TcO₄⁻.³⁰ Other studies showed that iron metal, magnetite, and
200 adsorbed Fe(II) can effectively remove TcO₄⁻ from solution.^{27,52-56} Recovery of Tc from the
201 spinel ferrites was determined during analysis of Fe(II) and total iron (ΣFe) by determining the
202 amount of ⁹⁹Tc using LSC. The recovery of Tc varied from 81% to 100% (Table S1).

203

204 **X-ray diffraction (XRD).** Tc-doped spinel ferrites were characterized using XRD to determine
205 the oxide phases present, the lattice parameters, and the crystallite sizes of the major phase. XRD
206 patterns and Rietveld fits for the Tc-doped spinel ferrites are given in Figure 1. Samples prepared
207 by the coprecipitation route have broader peaks than samples produced by the oxidation route
208 due to the smaller crystallites produced by more rapid nucleation of nanoparticles in the
209 coprecipitation synthesis.⁵⁷ These results are consistent with the original magnetite syntheses
210 from which the procedures to prepare Tc-doped spinel ferrites were adapted.^{34,36} Undoped spinel
211 ferrites, prepared under identical conditions, but adding water instead of TcO_4^- , were also
212 characterized. These undoped samples allow the effect of Tc doping on the lattice parameters
213 and $\text{Fe(II)}/\Sigma\text{Fe}$ to be determined.

214



215
 216 **Figure 1:** X-ray powder patterns (in red) and Rietveld fits (black) of spinel ferrites. Data are
 217 normalized so that the largest peaks have the same height. Data for $Tc_{0.1}M_{0.2}Fe_{2.7}O_4$ are given in
 218 the SI and are similar to those of $Tc_{0.1}Fe_{2.9}O_4$. Impurity peaks are labeled with g for goethite, r
 219 for α -MnOOH, and d for the layered double hydroxide. Diffraction peaks of the coprecipitation
 220 samples are broader than those produced by the oxidation route due to the smaller crystallite
 221 sizes of the coprecipitation samples.

222
 223 The major phase was spinel ferrite in all samples. The most common impurity was goethite,
 224 which forms in the presence of oxygen.³⁶ Its presence suggests that the short sparging period did
 225 not remove all of the oxygen. When Mn(II) was used, α -MnOOH, was observed. When Ni(II)

226 was used, an impurity was indicated by broad peaks at $2\theta = 22.5^\circ$, 35° , and 60° , which is
227 consistent with the presence of a lamellar nickel/iron layered double hydroxide (LDH) phase.^{58,59}

228

229 **Effects of charge compensation on lattice parameters and Fe(II)/ Σ Fe ratio.** Tc-doping

230 affects the lattice parameters of the spinel ferrites (Figure 2), which provides information about

231 the mechanism that balances the charge mismatch created when Tc(IV) replaces Fe(III). While

232 other mechanisms are possible,³² the charge mismatch may be balanced in two main ways: M(II)

233 could replace Fe(III) (divalent substitution) or one vacancy at a Fe(III) site could be created for

234 every three Tc(IV) (maghemitization). In TiFe_2O_4 (ulvöspinel), the charge mismatch is balanced

235 by divalent substitution leading to a lattice expansion to 8.521 Å relative to magnetite, 8.397 Å.⁴⁵

236 Lattice expansion occurs because M(II) ions are larger than the Fe(III) that they replace. In

237 contrast, maghemitization decreases the lattice parameter, i.e. to 8.341 Å in of Ti-doped

238 maghemite, $\text{Ti}_{0.42}\text{Fe}_{2.18}\text{O}_4$.⁶⁰ Previous studies of iron oxides doped with tetravalent ions suggest

239 that divalent substitution occurs under reducing conditions and maghemitization occurs under

240 oxidizing conditions.⁶¹⁻⁶⁴

241

242 The lattice parameters of the Tc-doped and undoped spinel ferrites are compared in Figure 2. To

243 explain the results, the samples are categorized by the amount of M(II) and Fe(II) present during

244 synthesis. Samples prepared by the oxidation route are “high Fe(II)” while coprecipitation

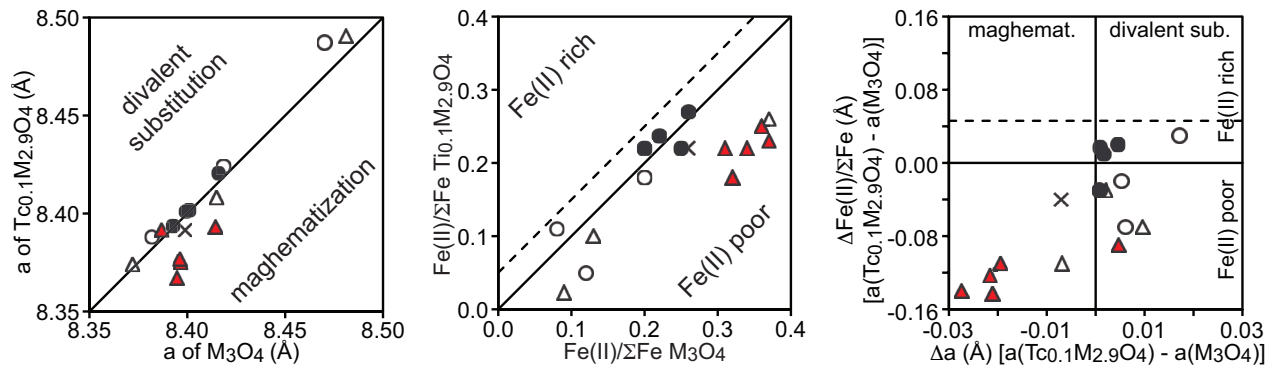
245 samples are “low Fe(II)”. Spinel ferrites, $\text{Tc}_{0.1}\text{M}_{1.1}\text{Fe}_{1.8}\text{O}_4$, are “high M(II),” and doped magnetite

246 samples, $\text{Tc}_{0.1}\text{M}_{0.2}\text{Fe}_{2.7}\text{O}_4$, are “low M(II).” For example, $\text{Tc}_{0.1}\text{Co}_{1.1}\text{Fe}_{1.8}\text{O}_4\text{-c}$ is high M(II), low

247 Fe(II). In samples with high M(II) and/or high Fe(II), Tc-doping increases the lattice parameters

248 with the exception of $\text{Tc}_{0.1}\text{Co}_{1.1}\text{Fe}_{1.8}\text{O}_4\text{-c}$ and $\text{Tc}_{0.1}\text{Fe}_{2.9}\text{O}_4\text{-o}$. The increased lattice parameter in

249 these samples suggests that charge is mainly balanced by divalent substitution, which is
 250 consistent with the large excess of divalent metal ions, either M(II) or Fe(II), present during
 251 these syntheses. On the other hand, except for $Tc_{0.1}Ni_{0.2}Fe_{2.7}O_4-c$ and $Tc_{0.1}Mn_{0.2}Fe_{2.7}O_4-c$,
 252 samples with low M(II) and low Fe(II) show a decrease in the lattice parameter upon Tc-doping.
 253 This decrease suggests that the charge mismatch is predominantly balanced by maghemitization,
 254 which is consistent with the smaller amounts of divalent metal ions present during synthesis.



255 **Figure 2.** (Left panel) comparison of lattice parameters of Tc doped spinel ferrites (vertical axis)
 256 with the lattice parameters of undoped samples (horizontal axis) (left). (Center) comparison of
 257 the Fe(II)/total Fe values for Tc-doped spinel ferrites (vertical axis) with the undoped analogs
 258 (horizontal axis). (Right) Change in Fe(II)/ ΣFe (vertical axis) and lattice parameter (horizontal
 259 axis) as a result of Tc-doping. The dashed line indicates the Fe(II)/total Fe value for a Tc-doped
 260 spinel ferrite if the charge is balanced by replacing Fe(III) by Fe(II). Open circles:
 261 $Tc_{0.1}M_{1.1}Fe_{1.8}O_4-o$ (high M(II), high Fe(II)). Filled circles: $Tc_{0.1}M_{0.2}Fe_{2.7}O_4-o$ (low M(II), high
 262 Fe(II)). Open triangles: $Tc_{0.1}M_{1.1}Fe_{1.8}O_4-c$ (high M(II), low Fe(II)). Filled triangles:
 263 $Tc_{0.1}M_{0.2}Fe_{2.7}O_4-c$ (low M(II), low Fe(II)).

264

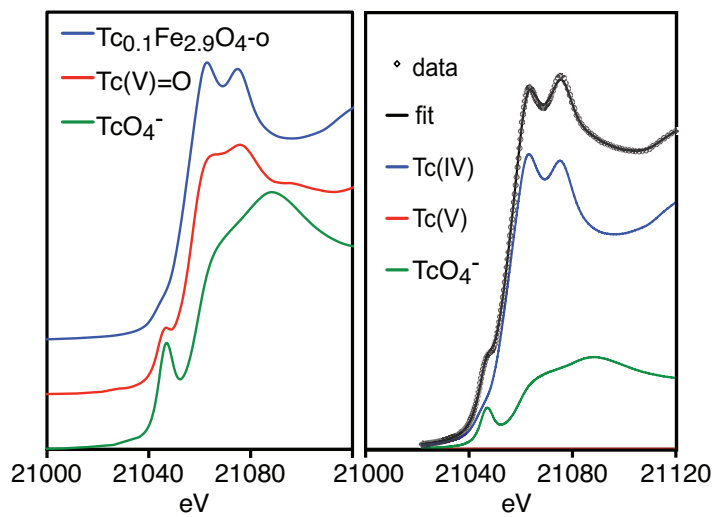
265 The XRD data suggests that the charge mismatch created by Tc doping is predominantly
 266 balanced by divalent substitution in high Fe(II) or high M(II) samples. The identity of the

267 divalent cation may be inferred from the ratio of Fe(II) to total iron (Fe(II)/ Σ Fe) (Table S1 and
268 Figure 2). If the divalent cation is Fe(II), Fe(II)/ Σ Fe will increase upon Tc doping as determined
269 by stoichiometry (dashed lines in Figure 2 for $\text{Tc}_{0.1}\text{Fe}_{2.9}\text{O}_4$). With some exceptions, Fe(II)/ Σ Fe is
270 smaller for Tc-doped samples, indicating that M(II) rather than Fe(II) replaces Fe(III) during
271 divalent substitution in the high M(II) samples. The relationship between the change in lattice
272 parameter and change in Fe(II)/ Σ Fe is illustrated in the right panel of Figure 2. In the low M(II)
273 samples (filled symbols) the changes in lattice parameter and Fe(II)/ Σ Fe are generally correlated
274 since either Fe(II) replaces Fe(III) to balance the charge and expand the lattice or the samples are
275 maghemitized and the lattice shrinks. High M(II) samples show less correlation because
276 replacing Fe(III) by M(II) expands the lattice but has little effect on Fe(II)/ Σ Fe.

277

278 **XAFS results.** Representative Tc K-edge XANES and EXAFS spectra are shown in Figures 3
279 and 4, respectively (the other EXAFS spectra are similar to $\text{Tc}_{0.1}\text{Fe}_{2.9}\text{O}_4\text{-o}$ and are included in the
280 SI). The model used to fit the EXAFS spectra is the octahedral site (M_O) of titanomagnetite
281 ($\text{Ti}_{0.1}\text{Fe}_{2.9}\text{O}_4$) occupied by Ti(IV). Tc(IV) and Ti(IV) are similar in size, so the local structure of
282 Ti(IV) in the M_O site is an appropriate model for the structure of Tc(IV) in spinel ferrites.
283 Coordination numbers for the metal neighbors were fixed at the value in the crystal structure, e.g.
284 6 nearest octahedral site (M_O) neighbors. A minor contribution from a short Tc-O distance at
285 either $<1.7 \text{ \AA}$ or $\sim 1.72 \text{ \AA}$ was used to obtain the best fit (Table 1). The 1.72 \AA Tc-O distance is
286 consistent with TcO_4^- .⁶⁵ The shorter Tc-O distance is ascribed to a fitting artifact. In some cases,
287 the shorter Tc-O distance is consistent with the distance of a terminal oxo group of Tc(V), 1.64
288 \AA .⁶⁶ However, the shorter Tc-O distance varies widely from 1.51 \AA to 1.69 \AA . This variation is
289 inconsistent with the presence of a well-defined Tc(V) species for which the same Tc-O distance

290 should be observed in all samples as seen in the samples that contain TcO_4^- . Moreover, XANES
291 analysis, Table 1, does not confirm the presence Tc(V) in any of the samples with very short Tc-
292 O distances. Only two samples contain Tc(V) greater than 3σ in the XANES analysis:
293 $\text{Tc}_{0.1}\text{Mn}_{1.1}\text{Fe}_{1.8}\text{O}_{4-\text{c}}$ and $\text{Tc}_{0.1}\text{Ni}_{1.1}\text{Fe}_{1.8}\text{O}_{4-\text{c}}$, and both have Tc-O bond distances consistent with
294 TcO_4^- . In contrast, EXAFS and XANES analysis show better agreement for TcO_4^- . In all cases
295 but one, TcO_4^- is found in materials produced by the low Fe(II), coprecipitation route. For most
296 samples produced by the oxidation route, the only significant oxidation state is Tc(IV) ,
297 presumably due to the large excess of Fe(II) used in these syntheses. Based on the XANES
298 analyses, the main oxidation state of Tc in all samples is Tc(IV) although some contain TcO_4^- .
299



300
301 **Figure 3.** XANES standard spectra (left) and deconvoluted XANES fit for $\text{Tc}_{0.1}\text{Co}_{1.1}\text{Fe}_{1.8}\text{O}_{4-\text{c}}$
302 (right).
303

304 **Table 1:** Tc oxidation state distribution from EXAFS and XANES analyses

Sample ^a	Tc-O (Å) (EXAFS)	# short Tc-O ^b (EXAFS)	TcO ₄ ^{-c} (EXAFS)	Tc(IV) (XANES)	Tc(V) ^d (XANES)	TcO ₄ ⁻ (XANES)
Tc _{0.1} Mn _{1.1} Fe _{1.8} O _{4-o}	1.59(1)	0.28(8)	--	1.0(1)	0.0(2)	0.00(6)
Tc _{0.1} Co _{1.1} Fe _{1.8} O _{4-o}	1.54(3)	0.3(1)	--	1.0(1)	0.0(2)	0.00(6)
Tc _{0.1} Ni _{1.1} Fe _{1.8} O _{4-o}	1.79(3)	--	0.10(2)	0.96(8)	0.0(1)	0.04(4)
Tc _{0.1} Mg _{0.2} Fe _{2.7} O _{4-o}	1.54(2)	0.29(9)	--	1.00(9)	0.0(1)	0.00(4)
Tc _{0.1} Mn _{0.2} Fe _{2.7} O _{4-o}	1.51(1)	0.38(9)	--	0.93(5)	0.00(8)	0.07(3)
Tc _{0.1} Fe _{2.9} O _{4-o}	1.61(2)	0.20(8)	--	1 ^e		
Tc _{0.1} Co _{0.2} Fe _{2.7} O _{4-o}	1.66(2)	0.4(1)	--	0.9(1)	0.0(2)	0.10(6)
Tc _{0.1} Ni _{0.2} Fe _{2.7} O _{4-o}	1.57(1)	0.31(8)	--	1.00(6)	0.0(1)	0.00(3)
Tc _{0.1} Mn _{1.1} Fe _{1.8} O _{4-c}	1.72(1)	--	0.10(2)	0.62(9)	0.4(1)	0.01(5)
Tc _{0.1} Co _{1.1} Fe _{1.8} O _{4-c}	1.718(5)	--	0.21(2)	0.75(5)	0.00(7)	0.25(3)
Tc _{0.1} Ni _{1.1} Fe _{1.8} O _{4-c}	1.726(6)		0.30(2)	0.54(3)	0.24(5)	0.22(2)
Tc _{0.1} Mg _{0.2} Fe _{2.7} O _{4-c}	1.671(6)	0.33(8)	--	0.84(3)	0.11(4)	0.06(1)
Tc _{0.1} Mn _{0.2} Fe _{2.7} O _{4-c}	1.715(7)		0.18(2)	0.80(3)	0.04(4)	0.16(2)
Tc _{0.1} Fe _{2.9} O _{4-c}	1.63(1)	0.29(6)	--	0.89(3)	0.09(5)	0.03(2)
Tc _{0.1} Co _{0.2} Fe _{2.7} O _{4-c}	1.716(9)		0.19(2)	0.82(3)	0.01(4)	0.17(1)
Tc _{0.1} Ni _{0.2} Fe _{2.7} O _{4-c}	1.720(8)		0.15(2)	0.82(2)	0.00(3)	0.18(1)

- 305 a) Samples with an “o” suffix were prepared by oxidation; “c” by coprecipitation
306 b) Coordination number of the O neighbors with a Tc-O distance <1.7 Å.
307 c) Fraction of TcO₄⁻ is ¼ of the number of O neighbors with a Tc-O distance between 1.7
308 and 1.8 Å.
309 d) Relative to sample Tc_{0.1}Fe_{2.9}O_{4-o}.
310 e) The XANES spectrum of this sample is the Tc(IV) standard.
311

312

313

314

Table 2. Local environment of Tc in spinel ferrites from EXAFS^{a,b}

Sample ^a	6 O (Å)	σ^2 (Å ²)	6 M _O (Å) ^c	# of Tc ^d	σ^2 (Å ²)	6 M _T (Å) ^e	σ^2 (Å ²)	12 M _O (Å) ^b
M _O site in Fe ₃ O ₄	2.06	--	2.97	--	--	3.48	--	5.15
M _O site in TiFe ₂ O ₄ ⁴⁵	2.09	--	3.02	--	--	3.54	--	5.22
High M(II), High Fe(II)								
Tc _{0.1} Mn _{1.1} Fe _{1.8} O _{4-o}	2.025(3)	0.004	3.087(7)	2.0(1)	0.004	3.565(8)	0.013	5.27(2)
Tc _{0.1} Co _{1.1} Fe _{1.8} O _{4-o}	2.009(4)	0.003	3.035(5)	0 ^f	0.006	3.517(7)	0.006	5.19(1)
Tc _{0.1} Ni _{1.1} Fe _{1.8} O _{4-o}	2.009(4)	0.003	3.034(6)	1.2(5)	0.003	3.514(7)	0.007	5.19(1)
Low M(II), High Fe(II)								
Tc _{0.1} Mg _{0.2} Fe _{2.7} O _{4-o}	2.034(4)	0.003	3.096(9)	1.9(2)	0.004	3.537(7)	0.007	5.22(2)
Tc _{0.1} Mn _{0.2} Fe _{2.7} O _{4-o}	2.036(4)	0.004	3.100(8)	2.20(8)	0.002	3.53(1)	0.010	5.25(2)
Tc _{0.1} Fe _{2.9} O _{4-o}	2.027(3)	0.004	3.090(7)	2.1(1)	0.004	3.524(6)	0.008	5.22(2)
Tc _{0.1} Co _{0.2} Fe _{2.7} O _{4-o}	2.026(6)	0.005	3.08(1)	2.2(1)	0.003	3.51(1)	0.008	5.20(2)
Tc _{0.1} Ni _{0.2} Fe _{2.7} O _{4-o}	2.030(3)	0.003	3.075(7)	1.9(1)	0.003	3.530(6)	0.007	5.21(1)
High M(II), Low Fe(II)								
Tc _{0.1} Mn _{1.1} Fe _{1.8} O _{4-c}	2.016(5)	0.004	3.083(1)	2.0(2)	0.003	3.550(3)	0.015	5.26(4)
Tc _{0.1} Co _{1.1} Fe _{1.8} O _{4-c}	2.027(5)	0.004	3.069(8)	2.07(8)	0.001	3.54(1)	0.011	5.23(2)
Tc _{0.1} Ni _{1.1} Fe _{1.8} O _{4-c}	2.027(8)	0.006	3.10(2)	2.3(2)	0.005	3.50(3)	0.018	f
Low M(II), Low Fe(II)								
Tc _{0.1} Mg _{0.2} Fe _{2.7} O _{4-c}	2.027(8)	0.005	3.10(2)	2.27(8)	0.003	3.51(3)	0.012	5.23(1)
Tc _{0.1} Mn _{0.2} Fe _{2.7} O _{4-c}	2.019(4)	0.005	3.083(7)	2.10(8)	0.003	3.509(9)	0.012	5.23(2)
Tc _{0.1} Fe _{2.9} O _{4-c}	2.020(3)	0.005	3.086(6)	2.17(6)	0.002	3.511(8)	0.011	5.23(2)
Tc _{0.1} Co _{0.2} Fe _{2.7} O _{4-c}	2.020(5)	0.005	3.077(9)	2.16(9)	0.003	3.51(1)	0.011	5.22(2)
Tc _{0.1} Ni _{0.2} Fe _{2.7} O _{4-c}	2.019(5)	0.005	3.074(9)	1.93(4)	0.004	3.509(9)	0.011	5.21(2)

315

a)

316

b) Standard deviations are given in parentheses in the same units as the last digit

317

c) M_O: octahedral sites

318

d) # of nearest octahedral neighbor that are Tc rather than Fe, Mg, Mn, Co, Ni

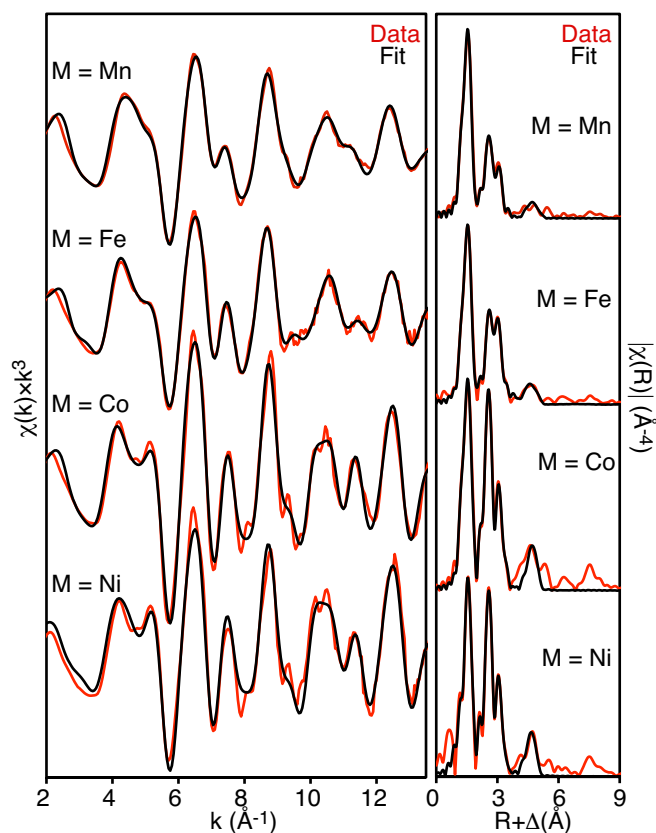
319

e) M_T: tetrahedral sites

320

f) Inclusion of this set of atoms did not improve the fit.

321



322
 323 **Figure 4.** Tc K-edge EXAFS spectra of $\text{Tc}_{0.1}\text{M}_{1.1}\text{Fe}_{1.8}\text{O}_{4-o}$ (left) and Fourier transforms (right).
 324 Data are shown in color and EXAFS fits are shown in black. The spectra of $\text{Tc}_{0.1}\text{M}_{0.2}\text{Fe}_{2.7}\text{O}_4$ are
 325 similar to that labeled $M = \text{Fe}$.

326
 327 The EXAFS results, Table 2, are consistent with the bulk of Tc in the sample existing as Tc(IV)
 328 occupying the octahedral spinel site (M_{O}) site as previously seen for Tc-doped magnetite.^{27,31}
 329 The local environment of Tc is more similar to the M_{O} site of ulvöspinel (TiFe_2O_4) than that of
 330 Fe_3O_4 as shown in Table 2. The oxygen neighbors at 2.0 \AA are characteristic for Tc(IV)
 331 octahedrally coordinated by oxygen.⁶⁷ The Tc and Fe atoms at 3.1 \AA are consistent with the six,
 332 edge-sharing M_{O} neighbors at 3.02 \AA in TiFe_2O_4 . The six Fe atoms at 3.5 \AA are in agreement
 333 with the six, corner-sharing M_{T} neighbors at 3.53 \AA in TiFe_2O_4 . Scattering from more distant
 334 iron M_{O} sites at 5.2 \AA was observed in most cases, which is consistent with the next-nearest

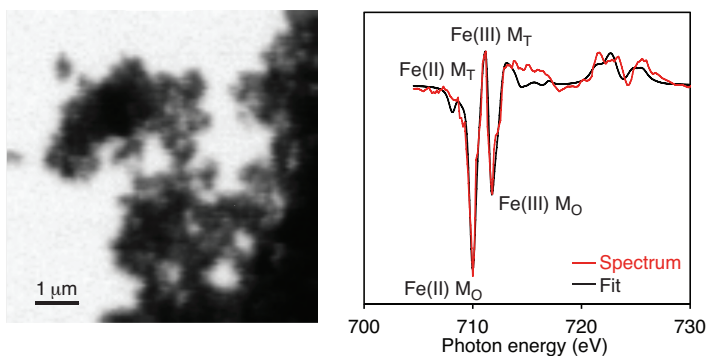
335 neighbor M_O sites at 5.22 Å in $TiFe_2O_4$. In some samples, scattering from more distant atoms can
336 be observed at ~ 8 Å in the Fourier transformed spectra, which presumably corresponds to 42 Fe
337 neighbors that are 7.9 and 8.2 Å from M_O . The presence of Fe and/or Tc neighbors²⁷ at 3.1 Å, 3.5
338 Å, and 5.2 Å is sufficient to show that the bulk of the Tc is doped into the M_O site. This result is
339 consistent with previous EXAFS studies of magnetite doped with Sn(IV) or Ti(IV) and to the
340 previously mentioned results for Tc(IV) doped magnetite.^{62,68,69}

341
342 The most surprising result is that Tc is strongly clustered, which was not previously observed,
343 presumably because the Tc/Fe ratio was much lower in those studies. At the doping level used
344 here, each Tc would have 0.3 Tc neighbors if Tc were homogeneously distributed. Instead, each
345 Tc has ~ 2 Tc neighbors. The local environment of Tc again resembles that of Ti in $TiFe_2O_4$
346 where each Ti has 3 Ti(IV) M_O neighbors, and the remaining M_O and M_T sites are occupied by
347 Fe(II). The level of Tc clustering in the Tc-doped spinel ferrites implies that the M_O sites
348 surrounding each Tc site contain approximately two Tc(IV) and four M(II) and that the
349 neighboring M_T sites contain approximately three Fe(III) and three M(II).

350
351 The distances determined by EXAFS are slightly different from those determined by
352 crystallography because EXAFS measures the local structure of Tc while XRD measures the
353 average structure. The 2.02 Å Tc-O distance is shorter than M_O -O distance in $TiFe_2O_4$, which
354 includes both Ti(IV)-O and Fe(II)-O distances. Using the ionic radius of four coordinate O^{2-}
355 (1.24 Å),²¹ the Tc-O distance is predicted to be 2.025 Å. In $TiFe_2O_4$, the average radius of M_O is
356 0.832 Å, and the predicted M_O -O distance is 2.07 Å. The longer Tc- M_O distance relative to
357 $TiFe_2O_4$ largely results from Tc clustering. Each Tc has ~ 2 Tc neighbors and ~ 4 M(II) neighbors.

358 In $\text{Tc}_{0.1}\text{Fe}_{2.9}\text{O}_{4-\delta}$, the average ionic radius of the M_O neighbors of Tc is 0.875 Å, about 0.04 Å
359 larger than in TiFe_2O_4 , so the Tc- M_O distance determined by EXAFS should be longer than that
360 determined by diffraction.

361
362 **Fe L-edge XMCD spectroscopy.** $\text{Tc}_{0.1}\text{Fe}_{2.9}\text{O}_{4-\delta}$ was studied using XMCD at the Fe $\text{L}_{2,3}$ -edge in
363 an attempt to determine the distribution of Fe(II) and Fe(III) on the octahedral and tetrahedral
364 sites. This technique has been widely used to study substituted magnetites including
365 titanomagnetites.^{50,51,68} The normal contrast X-ray image and the XMCD spectrum are shown in
366 Figure 5. The cation distribution from the fit, normalized for 2.9 Fe and an M_T occupancy of 1,
367 shows that the M_O sites contain 0.7 Fe(III) and 1.2 Fe(II) and M_T contains 1 Fe(III). This
368 occupancy is similar to that predicted if the charge is balanced by diamagnetic substitution (M_O
369 sites contain 0.1 Tc(IV), 0.8 Fe(III) and 1.1 Fe(II), and M_T sites contain 1 Fe(III)). The XMCD
370 results suggest a Fe(II)/ ΣFe ratio of 0.4, which is somewhat larger than measured
371 colorimetrically, 0.21(1).



372
 373 **Figure 5.** Normal contrast X-ray micrograph (STXM, left) of $\text{Tc}_{0.1}\text{Fe}_{2.9}\text{O}_{4-o}$ illustrating the small
 374 particle size. X-ray magnetic circular dichroism spectrum (XMCD, right) of $\text{Tc}_{0.1}\text{Fe}_{2.9}\text{O}_{4-o}$
 375 obtained at the Fe $L_{2,3}$ -edge. The XMCD spectrum is the difference between absorption of right
 376 and left circularly polarized X-rays when the sample is in a magnetic field.

377
 378 The Tc-doped spinel ferrites consist of Tc-rich regions and Tc-poor regions. This behavior
 379 closely mirrors that of titanomagnetite where Ti(IV) mainly replaces Fe(III) on M_O , and the
 380 charge is balanced by divalent substitution. Ti(IV) is homogeneously distributed above 600 °C.⁷⁰
 381 At lower temperatures, titanomagnetite undergoes spinodal decomposition forming titanium-
 382 poor regions that resemble magnetite and titanium-rich regions that resemble ulvöspinel.⁷⁰
 383 Recent work by Lilova, et al. shows that the enthalpy of mixing for the ulvöspinel/magnetite
 384 system is positive, consistent with the observed spinodal decomposition.⁷¹ The behavior of the
 385 Tc-doped spinel ferrites appears to be similar, and may explain why the local structure of Tc(IV)
 386 more closely resembles ulvöspinel than magnetite.

387
 388 **Implications for durability of Tc-doped spinels.** The spinel ferrites in this study are effective
 389 at stabilizing Tc(IV) in the solid state and preventing its oxidation to TcO_4^- . Only the initial step
 390 of the synthesis was performed under inert atmosphere. All subsequent operations, including

391 washing, storage, and spectroscopic studies, were performed in air. Nevertheless, Tc remained in
392 the reduced state. While the ability to stabilize Tc(IV) is necessary for these materials to be
393 effective waste forms for ⁹⁹Tc, the spinel ferrite matrix also must be sufficiently durable towards
394 dissolution or alteration.

395
396 The main concern, therefore, is the durability of the Tc-doped spinel ferrites. As prepared herein,
397 these materials are nanoparticles with high specific surface areas. In addition, the materials
398 contain Fe(II), which may adversely affect their durability. The effect of Fe(II) on durability is
399 best illustrated by magnetite and titanomagnetite. In aerobic environments, these materials are
400 oxidized to γ -Fe₂O₃ (maghemite) and titanomaghemite, respectively.^{69,72} This transformation is
401 topotactic and unlikely to release doped Tc, as observed by Marshall et al.³¹ While somewhat
402 durable, maghemite is unstable with respect to transformation to hematite or goethite. This
403 transformation is not topotactic and could lead to the loss of Tc to the environment. Work by
404 Um, et al. suggest that Tc(IV) can still be trapped in goethite during the oxidation of magnetite.^{28,29}
405 As in magnetite, the Fe(III) site in goethite is octahedral, and Tc(IV) can replace Fe(III) provided
406 that the charge mismatch is balanced. Ultimately, the best approach for determining how well
407 these materials immobilize ⁹⁹Tc is measuring the release of ⁹⁹Tc when these materials are re-
408 suspended in water.

409
410

411 **Acknowledgement**

412 This work (WWL, DKS, NM) was supported by the U.S. Department of Energy, Office of
413 Science, Basic Energy Sciences, Chemical Sciences, Biosciences, and Geosciences Division

414 (CSGB), Heavy Element Chemistry Program and was performed at Lawrence Berkeley National
415 Laboratory under contract No. DE-AC02-05CH11231. CIP was supported by the Geosciences
416 Group at Pacific Northwest National Laboratory. Tc K-edge XAFS spectra were obtained at the
417 Stanford Synchrotron Radiation Lightsource, SLAC National Accelerator Laboratory, which is
418 supported by the U.S. Department of Energy, Office of Science, Office of Basic Energy Sciences
419 under Contract No. DE-AC02-76SF00515. STXM and XMCD data were obtained at Beamline
420 11.0.2 at the ALS, which is supported by the Director, Office of Science, Office of Basic Energy
421 Sciences, CSGB Condensed Phase and Interfacial Molecular Sciences program, of the U.S.
422 Department of Energy at Lawrence Berkeley National Laboratory under Contract No. DE-AC02-
423 05CH11231. The ALS and TT are supported by the Director, Office of Science, Office of Basic
424 Energy Sciences, of the U.S. Department of Energy under Contract No. DE-AC02-05CH11231.

425

426 **Supplemental Information.** XANES spectra, larger diffraction patterns, larger EXAFS spectra
427 and detailed fitting results, and combined analytical data are given in the SI.

428

429 **References**

- 430 (1) Icenhower, J. P.; Qafoku, N. P.; Zachara, J. M.; Martin, W. J. The biogeochemistry of
431 technetium: a review of the behavior of an artificial element in the natural environment. *Am. J.*
432 *Sci.* **2010**, *310*, 721.
- 433 (2) Pilkington, N. J. The solubility of technetium in the near-field environment of a
434 radioactive-waste repository. *J. Less Common Met.* **1990**, *161*, 203.
- 435 (3) Kunze, S.; Neck, V.; Gompper, K.; Fanghanel, T. Studies on the immobilization of
436 technetium under near field geochemical conditions. *Radiochim. Acta* **1996**, *74*, 159.
- 437 (4) Ishii, T.; Sakuragi, T. Technetium in the environment. *Radioisotopes* **2006**, *55*, 485.
- 438 (5) *Yucca Mountain Repository License Application*, DOE/RW-0573, Rev. 0, U.S.
439 Department of Energy, 2008.
- 440 (6) Mann, F. M.; Puigh, R. J.; Finfrock, S. H.; Khaleel, R.; Wood, M. I. *Integrated Disposal*
441 *Facility Risk Assessment*, RPP-15834, CH2M Hill Hanford Group, Inc., 2003.
- 442 (7) *Performance Assessment for the Saltstone Disposal Facility at the Savannah River Site*,
443 SRR-CWDA-2009-00017, SRR Closure & Waste Disposal Authority, 2009.

- 444 (8) *EPA facts about Technetium-99*, U.S. Environmental Protection Agency, 2014.
- 445 (9) Liu, D. J.; Yao, J.; Wang, B.; Bruggeman, C.; Maes, N. Solubility study of Tc(IV) in a
446 granitic water. *Radiochim. Acta* **2007**, *95*, 523.
- 447 (10) Hess, N. J.; Xia, Y. X.; Rai, D.; Conradson, S. D. Thermodynamic model for the
448 solubility of $\text{TcO}_2 \cdot x\text{H}_2\text{O}(\text{am})$ in the aqueous $\text{Tc}(\text{IV})\text{-Na}^+\text{-Cl}^-\text{-H}^+\text{-OH}^-\text{-H}_2\text{O}$ system. *J. Solution*
449 *Chem.* **2004**, *33*, 199.
- 450 (11) Gu, B. H.; Dong, W. M.; Liang, L. Y.; Wall, N. A. Dissolution of technetium(IV) oxide
451 by natural and synthetic organic ligands under both reducing and oxidizing conditions. *Environ.*
452 *Sci. Technol.* **2011**, *45*, 4771.
- 453 (12) Boggs, M. A.; Minton, T.; Dong, W. M.; Lomasney, S.; Islam, M. R.; Gu, B. H.; Wall, N.
454 A. Interactions of Tc(IV) with humic substances. *Environ. Sci. Technol.* **2011**, *45*, 2718.
- 455 (13) Sekine, T.; Watanabe, A.; Yoshihara, K.; Kim, J. I. Complexation of technetium with
456 humic acid. *Radiochim. Acta* **1993**, *63*, 87.
- 457 (14) Yalcintas, E.; Gaona, X.; Altmaier, M.; Dardenne, K.; Polly, R.; Geckeis, H.
458 Thermodynamic description of Tc(IV) solubility and hydrolysis in dilute to concentrated NaCl,
459 MgCl_2 and CaCl_2 solutions. *Dalton Trans.* **2016**, *45*.
- 460 (15) Migge, H. Simultaneous evaporation of Cs and Tc during vitrification-a thermochemical
461 approach. *Mater. Res. Soc. Symp. Proc.* **1990**, *176*, 411.
- 462 (16) Lammertz, H.; Merz, E.; Halaszovich, S. Technetium volatilization during HLW
463 vitrification. *Mater. Res. Soc. Symp. Proc.* **1985**, *44*, 823.
- 464 (17) Bibler, N. E.; Fellingner, T. L.; Marra, S. L.; O'Driscoll, R. J.; Ray, J. W.; Boyce, W. T.
465 Tc-99 and Cs-137 volatility from the DWPF production melter during vitrification of the first
466 macrobatch of HLW sludge at the Savannah River Site. *Mater. Res. Soc. Symp. Proc.* **2000**, *608*,
467 697.
- 468 (18) Lee, M.-S.; Um, W.; Wang, G.; Kruger, A. A.; Lukens, W. W.; Rousseau, R.; Glezakou,
469 V.-A. Impeding $^{99}\text{Tc}(\text{IV})$ mobility in novel waste forms. *Nature Commun.* **2016**, *7*, 12067.
- 470 (19) Ringwood, A. E.; Kesson, S. E.; Ware, N. G.; Hibberson, W.; Major, A. Immobilization
471 of high-level nuclear reactor wastes in Synroc. *Nature* **1979**, *278*, 219.
- 472 (20) Muller, O.; White, W. B.; Roy, R. Crystal chemistry of some technetium-containing
473 oxides. *J. Inorg. Nucl. Chem.* **1964**, *26*, 2075.
- 474 (21) Shannon, R. D. Revised effective ionic-radii and systematic studies of interatomic
475 distances in halides and chalcogenides. *Acta Cryst. A* **1976**, *32*, 751.
- 476 (22) Edouminko, A.; Colin, F.; Trescases, J. J. Alterability of titanium minerals (ilmenite and
477 rutile) and titanium mobility in the weathering profiles of the Ouala sector (Gabon). *J. Afr. Earth*
478 *Sci.* **1995**, *21*, 313.
- 479 (23) Ramanaidou, E.; Nahon, D.; Decarreau, A.; Melfi, A. J. Hematite and goethite from
480 duricrusts developed by lateritic chemical weathering of Precambrian banded iron formations,
481 Minas Gerais, Brazil. *Clay Clay Miner.* **1996**, *44*, 22.
- 482 (24) Shuster, D. L.; Vasconcelos, P. M.; Heim, J. A.; Farley, K. A. Weathering geochronology
483 by (U-Th)/He dating of goethite. *Geochim. Cosmochim. Acta* **2005**, *69*, 659.
- 484 (25) Yapp, C. J. Climatic implications of surface domains in arrays of SD and delta O-18 from
485 hydroxyl minerals: goethite as an example. *Geochim. Cosmochim. Acta* **2000**, *64*, 2009.
- 486 (26) Skomurski, F. N.; Rosso, K. M.; Krupka, K. M.; McGrail, B. P. Technetium
487 incorporation into hematite ($\alpha\text{-Fe}_2\text{O}_3$). *Environ. Sci. Technol.* **2010**, *44*, 5855.

- 488 (27) Kobayashi, T.; Scheinost, A. C.; Fellhauer, D.; Gaona, X.; Altmaier, M. Redox behavior
489 of Tc(VII)/Tc(IV) under various reducing conditions in 0.1 M NaCl solutions. *Radiochim. Acta*
490 **2013**, *101*, 323.
- 491 (28) Um, W.; Chang, H. S.; Icenhower, J. P.; Lukens, W. W.; Serne, R. J.; Qafoku, N. P.;
492 Westsik, J. H.; Buck, E. C.; Smith, S. C. Immobilization of 99-technetium (VII) by Fe(II)-
493 goethite and limited reoxidation. *Environ. Sci. Technol.* **2011**, *45*, 4904.
- 494 (29) Um, W.; Chang, H.; Icenhower, J. P.; Lukens, W. W.; Serne, R. J.; Qafoku, N.;
495 Kukkadapu, R. K.; Westsik, J. H. Iron oxide waste form for stabilizing Tc-99. *J. Nucl. Mat.*
496 **2012**, *429*, 201.
- 497 (30) Pepper, S. E.; Bunker, D. J.; Bryan, N. D.; Livens, F. R.; Charnock, J. M.; Pattrick, R. A.
498 D.; Collison, D. Treatment of radioactive wastes: an X-ray absorption spectroscopy study of the
499 reaction of technetium with green rust. *J. Colloid Interface Sci.* **2003**, *268*, 408.
- 500 (31) Marshall, T. A.; Morris, K.; Law, G. T. W.; Mosselmans, J. F. W.; Bots, P.; Parry, S. A.;
501 Shaw, S. Incorporation and retention of 99-Tc(IV) in magnetite under high pH conditions.
502 *Environ. Sci. Technol.* **2014**, *48*, 11853.
- 503 (32) Smith, F. N.; Um, W.; Taylor, C. D.; Kim, D.-S.; Schweiger, M. J.; Kruger, A. A.
504 Computational investigation of technetium(IV) incorporation into inverse spinels: magnetite
505 (Fe_3O_4) and trevorite (NiFe_2O_4). *Environ. Sci. Technol.* **2017**, *50*, 5216.
- 506 (33) Bohor, B. F.; Foord, E. E.; Ganapathy, R. Magnesioferrite from the Cretaceous-Tertiary
507 boundary, Caravaca, Spain. *Earth Planet. Sci. Lett.* **1986**, *81*, 57.
- 508 (34) Tang, Z. X.; Sorensen, C. M.; Klabunde, K. J.; Hadjipanayis, G. C. Preparation of
509 manganese ferrite fine particles from aqueous solution. *J. Colloid. Interface. Sci.* **1991**, *146*, 38.
- 510 (35) Kodama, T.; Wada, Y.; Yamamoto, T.; Tsuji, M.; Tamaura, Y. Synthesis and
511 characterization of ultrafine nickel(II)-bearing ferrites ($\text{Ni}_x\text{Fe}_{3-x}\text{O}_4$, $X=0.14-1.0$). *J. Mater. Chem.*
512 **1995**, *5*, 1413.
- 513 (36) Sugimoto, T.; Matijevic, E. Formation of uniform spherical magnetite particles by
514 crystallization from ferrous hydroxide gel. *J. Colloid Interface Sci.* **1980**, *74*, 227.
- 515 (37) Kaneko, K.; Katsura, T. Formation of Mg-bearing ferrite by the air oxidation of aqueous
516 suspensions. *Bull. Chem. Soc. Jpn.* **1979**, *52*, 747.
- 517 (38) Kiyama, M. Formation of manganese and cobalt ferrites by air oxidation of aqueous
518 suspensions and their properties. *Bull. Chem. Soc. Jpn.* **1978**, *51*, 134.
- 519 (39) Wilson, A. D. The micro-determination of ferrous iron in silicate minerals by a
520 volumetric and a colorimetric method. *Analyst* **1960**, *85*, 823.
- 521 (40) Whitehead, D.; Malik, S. A. Determination of ferrous and total iron in silicate rocks by
522 automated colorimetry. *Anal. Chem.* **1975**, *47*, 554.
- 523 (41) Koningsberger, D. C.; Prins, R. *X-Ray Absorption: Principles, Applications, Techniques*
524 *of EXAFS, SEXAFS, and XANES*; John Wiley & Sons: New York, 1988.
- 525 (42) Newville, M. IFEFFIT: interactive XAFS analysis and FEFF fitting. *J. Synchrotron Rad.*
526 **2001**, *8*, 322.
- 527 (43) Ravel, B. ATHENA and ARTEMIS interactive graphical data analysis using IFEFFIT.
528 *Phys. Scripta* **2005**, *T115*, 1007.
- 529 (44) Mustre de Leon, J.; Rehr, J. J.; Zabinsky, S. I.; Albers, R. C. Ab initio curved-wave x-
530 ray-absorption fine structure. *Phys. Rev. B* **1991**, *44*, 4146.
- 531 (45) Bosi, F.; Halenius, U.; Skogby, H. Crystal chemistry of the magnetite-ulvospinel series.
532 *Am. Mineral.* **2009**, *94*, 181.

- 533 (46) Downward, L.; Booth, C. H.; Lukens, W. W.; Bridges, F. A variation of the F-test for
534 determining statistical relevance of particular parameters in EXAFS fits. *AIP Conf. Proc.* **2007**,
535 882, 129.
- 536 (47) Bluhm, H.; Andersson, K.; Araki, T.; Benzerara, K.; Brown, G. E.; Dynes, J. J.; Ghosal,
537 S.; Gilles, M. K.; Hansen, H. C.; Hemminger, J. C.; Hitchcock, A. P.; Ketteler, G.; Kilcoyne, A.
538 L. D.; Kneedler, E.; Lawrence, J. R.; Leppard, G. G.; Majzlan, J.; Mun, B. S.; Myneni, S. C. B.;
539 Nilsson, A.; Ogasawara, H.; Ogletree, D. F.; Pecher, K.; Salmeron, M.; Shuh, D. K.; Tonner, B.;
540 Tyliczszak, T.; Warwick, T.; Yoon, T. H. Soft X-ray microscopy and spectroscopy at the
541 Molecular Environmental Science beamline at the Advanced Light Source. *J. Electron*
542 *Spectrosc. Relat. Phenom.* **2006**, 150, 86.
- 543 (48) van der Laan, G.; Kirkman, I. W. The 2p absorption spectra of 3d transition metal
544 compounds in tetrahedral and octahedral symmetry. *J. Phys. Condens. Matter* **1992**, 4, 4189.
- 545 (49) van der Laan, G.; Thole, B. T. Strong magnetic X-ray dichroism in 2p absorption spectra
546 of 3d transition metal ions. *Phys. Rev. B* **1991**, 43, 13401.
- 547 (50) Patrick, R. A. D.; Van der Laan, G.; Henderson, C. M. B.; Kuiper, P.; Dudzik, E.;
548 Vaughan, D. J. Cation site occupancy in spinel ferrites studied by X-ray magnetic circular
549 dichroism: developing a method for mineralogists. *Eur. J. Mineral.* **2002**, 14, 1095.
- 550 (51) Pearce, C. I.; Henderson, C. M. B.; Patrick, R. A. D.; Van der Laan, G.; Vaughan, D. J.
551 Direct determination of cation site occupancies in natural ferrite spinels by L₂,L₃ X-ray
552 absorption spectroscopy and X-ray magnetic circular dichroism. *Am. Mineral.* **2006**, 91, 880.
- 553 (52) Liang, L. Y.; Gu, B. H.; Yin, X. P. Removal of technetium-99 from contaminated
554 groundwater with sorbents and reductive materials. *Separ. Technol.* **1996**, 6, 111.
- 555 (53) Cui, D. Q.; Eriksen, T. E. Reduction of pertechnetate by ferrous iron in solution:
556 influence of sorbed and precipitated Fe(II). *Environ. Sci. Technol.* **1996**, 30, 2259.
- 557 (54) Peretyazhko, T.; Zachara, J. M.; Heald, S. M.; Jeon, B. H.; Kukkadapu, R. K.; Liu, C.;
558 Moore, D.; Resch, C. T. Heterogeneous reduction of Tc(VII) by Fe(II) at the solid-water
559 interface. *Geochim. Cosmochim. Acta* **2008**, 72, 1521.
- 560 (55) Peretyazhko, T.; Zachara, J. M.; Heald, S. M.; Kukkadapu, R. K.; Liu, C.; Plymale, A. E.;
561 Resch, C. T. Reduction of Tc(VII) by Fe(II) sorbed on Al (hydr)oxides. *Environ. Sci. Technol.*
562 **2008**, 42, 5499.
- 563 (56) Zachara, J. M.; Heald, S. M.; Jeon, B.-H.; Kukkadapu, R. K.; Liu, C.; McKinley, J. P.;
564 Dohnalkova, A. C.; Moore, D. A. Reduction of pertechnetate Tc(VII) by aqueous Fe(II) and the
565 nature of solid phase redox products. *Geochim. Cosmochim. Acta* **2007**, 71, 2137.
- 566 (57) Nguyen, T. K. T.; Maclean, N.; Mahiddine, S. Mechanisms of nucleation and growth of
567 nanoparticles in solution. *Chem. Rev.* **2014**, 114, 7610.
- 568 (58) Sasai, R.; Norimatsu, W.; Matsumoto, Y. Nitrate-ion-selective exchange ability of
569 layered double hydroxide consisting of Mg-II and Fe-II. *J. Hazard. Mat.* **2012**, 215, 311.
- 570 (59) Wang, Y.; Gao, H. Compositional and structural control on anion sorption capability of
571 layered double hydroxides (LDHs). *J. Colloid. Interface. Sci.* **2006**, 301, 19.
- 572 (60) Collyer, S.; Grimes, N. W.; Vaughan, D. J.; Longworth, G. Studies of the crystal-
573 structure and crystal-chemistry of titanomaghemite. *Am. Mineral.* **1988**, 73, 153.
- 574 (61) Berry, F. J.; Greaves, C.; Helgason, O.; McManus, J.; Palmer, H. M.; Williams, R. T.
575 Structural and magnetic properties of Sn-, Ti-, and Mg-substituted alpha-Fe₂O₃: A study by
576 neutron diffraction and Mossbauer spectroscopy. *J. Solid State Chem.* **2000**, 151, 157.

577 (62) Berry, F. J.; Bohorquez, A.; Helgason, O.; Jiang, J. Z.; McManus, J.; Moore, E.;
578 Mortimer, M.; Mosselmanns, F.; Morup, S. An investigation of the local environments of tin in
579 tin-doped alpha-Fe₂O₃. *J. Phys. Condens. Matter* **2000**, *12*, 4043.

580 (63) Berry, F. J.; Greaves, C.; Helgason, O.; McManus, J. Synthesis and characterization of
581 tin-doped iron oxides. *J. Mater. Chem.* **1999**, *9*, 223.

582 (64) Berry, F. J.; Skinner, S. J.; Helgason, O.; Bilsborrow, R.; Marco, J. F. Location of tin and
583 charge balance in materials of composition Fe_{3-x}Sn_xO₄ (x<0.3). *Polyhedron* **1998**, *17*, 149.

584 (65) Faggiani, R.; Lock, C. J. L.; Poce, J. Structure of ammonium pertechnetate at 295, 208
585 and 141 K. *Acta Crystallogr. Sect. B-Struct. Commun.* **1980**, *36*, 231.

586 (66) McGregor, D.; Burton-Pye, B. P.; Howell, R. C.; Mbomekalle, I. M.; Lukens, W. W.;
587 Bian, F.; Mausolf, E.; Poineau, F.; Czerwinski, K. R.; Francesconi, L. C. Synthesis, structure
588 elucidation, and redox properties of Tc-99 complexes of lacunary Wells-Dawson
589 polyoxometalates: insights into molecular Tc-99-metal oxide interactions. *Inorg. Chem.* **2011**,
590 *50*, 1670.

591 (67) Lukens, W. W.; Bucher, J. J.; Edelstein, N. M.; Shuh, D. K. Products of pertechnetate
592 radiolysis in highly alkaline solution: Structure of TcO₂•xH₂O. *Environ. Sci. Technol.* **2002**, *36*,
593 1124.

594 (68) Pearce, C. I.; Henderson, C. M. B.; Telling, N. D.; Pattrick, R. A. D.; Charnock, J. M.;
595 Coker, V. S.; Arenholz, E.; Tuna, F.; van der Laan, G. Fe site occupancy in magnetite-ulvospinel
596 solid solutions: A new approach using X-ray magnetic circular dichroism. *Am. Mineral.* **2010**,
597 *95*, 425.

598 (69) Pearce, C. I.; Qafoku, O.; Liu, J.; Arenholz, E.; Heald, S. M.; Kukkadapu, R. K.; Gorski,
599 C. A.; Henderson, C. M. B.; Rosso, K. M. Synthesis and properties of titanomagnetite (Fe₃₋
600 _xTi_xO₄) nanoparticles: A tunable solid-state Fe(II/III) redox system. *J. Colloid Interface Sci.*
601 **2012**, *387*, 24.

602 (70) Smith, P. P. K. Spinodal decomposition in a titanomagnetite. *Am. Mineral.* **1980**, *65*,
603 1038.

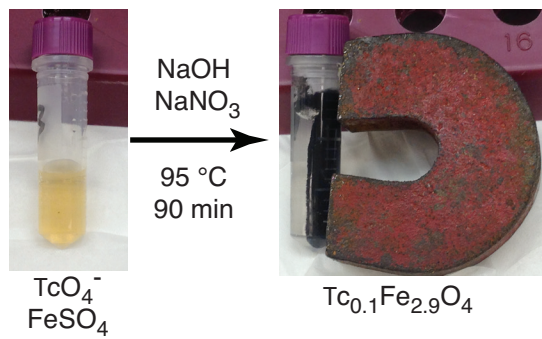
604 (71) Lilova, K. I.; Pearce, C. I.; Rosso, K. M.; Navrotsky, A. Energetics of spinels in the Fe-
605 Ti-O system at the nanoscale. *Chem. Phys. Chem.* **2014**, *15*, 3655.

606 (72) Pearce, C. I.; Liu, J.; Baer, D. R.; Qafoku, O.; Heald, S. M.; Arenholz, E.; Grosz, A. E.;
607 McKinley, J. P.; Resch, C. T.; Bowden, M. E.; Engelhard, M. H.; Rosso, K. M. Characterization
608 of natural titanomagnetites (Fe_{3-x}Ti_xO₄) for studying heterogeneous electron transfer to Tc(VII)
609 in the Hanford subsurface. *Geochim. Cosmochim. Acta* **2014**, *128*, 114.

610

611 TOC Figure:

612



613

614

615

616

617

618